Chinese Journal of Electronics
Vol.16, No.1, Jan. 2007

Automatic Change Detection from SAR Images Based on Fuzzy Entropy Principle*

PAN Chunhong, PRINET Veronique, YANG Qing and MA Songde

(*National Laboratory of Pattern Recognition, Institute of Automation, Chinese Academy of Sciences, Beijing 100080, China*)

Abstract — In this paper, we propose a general framework for automatic change detection of flooded areas in bi-temporal Synthetic aperture radar (SAR) imagery. Based on the fuzzy entropy principle, a single thresholding method is proposed. The difference image which is generated by subtracting, one SAR image from the other one, pixel by pixel, can be divided into two classes: changed and unchanged. Due to noise, this single threshold decision procedure applied in the difference image is prone to two kinds of errors: false positives and false negatives. To cope with this problem, the threshold method is performed again on the two separate classes. As a result, the difference image can be divided into changed, unchanged, and unlabelled classes. The unlabelled class contains most of the ambiguous pixels that are responsible for false positive and false negative errors. In order to identify the true category of the pixels in this class, we adopt a voting procedure to compute the saliency of each unlabelled candidate pixel by analyzing the region configuration in the local neighborhood. Finally, according to the radiometric characteristics of water bodies in SAR images, some verification measures are carried out to identify water changes.

Key words — Change detection, Fuzzy entropy, Voting, Homogeneous regions, Verification.

I. Introduction

With a large amount of satellite data available, there is an urgent need for change detection techniques that can automatically determine the locations of changes by comparing two images, which are taken from the same geographical area at difference times. The need stems from a wide range of applications such as: environmental monitoring[3], forest[6] and agricultural surveys[4], and so on.

Many methods have been proposed for automatic change detection[1,7,2] over the past two decades. Some comparative performance studies were reported in Refs.[8]. In Ref.[1], the authors used the Markov random field (MRF) method to model the spatial context in the prior model. Although this method exploited explicitly the local spatial information in the MRF framework, it did not make full use of all the information in the image. The preservation of MRF properties may not be guaranteed after some transformations such as subtraction of one image from another. To preserve the MRF property, one has to define a set of potential functions in the Gibbs energy function. However, only a simple potential function (the Kronecker delta function) was adopted in Ref.[1]. Thus the MRF properties may not be preserved in their framework. In Ref.[7], based on a global optimum strategy, the authors proposed an automatic change detection method. They used MRF to model the statistical correlation of intensity levels among neighbor pixels, and used a global optimum search to determine which class each pixel belongs to. The method was more accurate than pixel-based models to some extent. However, in their approach, they required some prior knowledge about the Gibbs potential and the Gibbs parameters, associated with the Gibbs potential for both noiseless image models and change image. This method is not practical in real applications. As a result, they had to make some assumptions on Gibbs potential when processing real images. It is obvious that the final result was excessively dependent on the form of the Gibbs potential. Furthermore, the optimal search was conducted over all pixels of the image. Although the Simulated annealing (SA) algorithm was used to reduce the complexity of the computation, this kind of search procedure was not feasible even with a normal size image, such as 512 by 512, because the complexity of computation increases rapidly according to image size.

In this paper, we propose a new method for automatic detection of changes in a water body by comparing two SAR images. In order to preserve the original image information, we analyze the difference image at two different levels instead of directly filtering speckle noise on two original images. Our method consists of three parts: First an entropy-based thresholding technique is used to analyze the difference image. To decrease the classification errors, we categorize the difference image into three classes: changed, unchanged, and unlabelled. Then for the unlabelled pixels, we compute their saliency by analyzing the contextual information in the local neighborhood. Finally, by using the radiometric properties of water bodies in SAR images, an effective verification is proposed to determine the water-inundated areas. Results with real images are included to demonstrate the validity of the proposed algorithm.

II. Classification of Difference Image

1. Thresholding based on fuzzy entropy principle

Image thresholding is an important technique in image processing and pattern recognition, which is regarded as the first step for image understanding. Many methods have been proposed to select the threshold automatically[12]. Let $D = \{d(i,j),(i,j) \in \boldsymbol{S}\}$ denote the intensity level of the difference image; here $\boldsymbol{S}$ is the dimension of the image. The change detection problem consists of determining a binary label $\phi(i,j)$ for each pixel on the difference image grid D. We associate $\phi(i,j)$ with two possible events: $\phi_u(i,j) = \textit{unchanged class}$, and $\phi_c(i,j) = \textit{changed class}$. Defining a threshold image T_o, and letting $\phi_{u,T}(i,j)$ and $\phi_{c,T}(i,j)$ denote the set of unchanged and changed classes induced by the threshold T, we have:

$$T_o = \begin{cases} \phi_{u,T}(i,j),(i,j) \in \boldsymbol{S}, & \text{if} \quad d(i,j) < T \\ \phi_{c,T}(i,j),(i,j) \in \boldsymbol{S}, & \text{otherwise} \end{cases}$$

Our objective is to find automatically a threshold T at which the difference image can be divided into two different classes based on its histogram. Let $\Omega = \{x_i; i = 1,2,\cdots,n\}$ be a fuzzy set with a

*Manuscript Received Sept. 2005; Accepted Mar. 2006.

membership function $\rho(x_i,T)$, where $x_i, i=1,2,\cdots,n$ are the possible outputs from source Ω with the probability $P(x_i)$. The fuzzy entropy of set Ω is defined as[10]:

$$J=-\sum_{x_i\in\Omega}P(x_i)\log P(x_i)\rho(x_i,T) \tag{1}$$

Entropy describes uniformity of the set Ω. When occurrence probabilities of different states x_i are uniform, the entropy of the set is high. If $\Omega=\{x_i;i=1,2,\cdots,n\}$ is viewed as the intensity levels of the difference image, then maximizing the fuzzy entropy defined in Eq.(1) is in fact to find any optimum threshold $\hat{T}$ to make the states x_i to be uniformly distributed in the set of Ω. When the membership function is moved pixel by pixel over the existing range of intensity levels, in each position, the fuzzy entropy is calculated. The position with a maximum amount of fuzzy entropy can be regarded as a suitable threshold. If the intensity level distribution of both changed class and unchanged class is the symmetrical one with a peak, intuitively the best theoretical threshold should be located at the intersection point of the two distributions. In other words, when the threshold T in the membership function corresponds to the theoretical optimum, the fuzzy entropy of the difference image reaches its maximum. Therefore, the Gaussian function can be selected as the membership function as follows:

$$\rho(x_i,T)=\frac{1}{\sqrt{2\pi}h}\exp\left\{-\frac{(x_i-T)^2}{2h^2}\right\} \tag{2}$$

We aim at obtaining an optimal threshold T to partition the difference image into two classes by maximizing the fuzzy entropy of the image:

$$J^*(\hat{T})=\arg\max_{T\in\Omega}\left\{-\sum_{x_i\in\Omega}P(x_i)\log P(x_i)\rho(x_i,T)\right\} \tag{3}$$

The optimal T should satisfy the following equation: $\partial J(T)/\partial T=0$, we have:

$$\begin{aligned}\frac{\partial J(T)}{\partial T}=&\frac{1}{\sqrt{2\pi}h^3}\sum_{x_i\in\Omega}P(x_i)\log P(x_i)\exp\left\{-\frac{(x_i-T)^2}{2h^2}\right\}\\&\cdot\left\{\frac{\sum_{x_i\in\Omega}x_iP(x_i)\log P(x_i)\exp\{-(x_i-T)^2/2h^2\}}{\sum_{x_i\in\Omega}P(x_i)\log P(x_i)\exp\{-(x_i-T)^2/2h^2\}}-T\right\}\\=&0\end{aligned} \tag{4}$$

where $\sum_{x_i\in\Omega}P(x_i)\log P(x_i)\exp\{-(x_i-T)^2/2h^2\}$ is a non-zero positive number. Since the solution to the equation cannot be directly computed, we use the iterative algorithm to find its solution. Therefore, Eq.(4) can be rewritten via iterative processes with:

$$T^{(j+1)}=\frac{\sum_{x_i\in\Omega}x_iP(x_i)\log P(x_i)\exp\{-(x_i-T^{(j)})^2/2h^2\}}{\sum_{x_i\in\Omega}P(x_i)\log P(x_i)\exp\{-(x_i-T^{(j)})^2/2h^2\}} \tag{5}$$

Let $c_i=P(x_i)\log P(x_i)$ and $K(\|x_i-T^{(j)}\|^2)=\exp\{-(x_i-T^{(j)})^2/2h^2\}$, the final iteration equation can be expressed as:

$$T^{(j+1)}=\frac{\sum_{x_i\in\Omega}c_ix_iK(\|x_i-T^{(j)}\|^2)}{\sum_{x_i\in\Omega}c_iK(\|x_i-T^{(j)}\|^2)} \tag{6}$$

where the superscripts j and $j+1$ denote the values of the parameters at the current and next iterations. From the above iteration equation, we obtain the sequences $\{T^{(j)}\}_{j=1,2,\cdots}$. It can be proved that the sequence $\{T^{(j)}\}_{j=1,2,\cdots}$ converges (Refer to Ref.[12] for detailed proof). The optimum threshold $\hat{T}$ would be obtained by determining whether the following equation is satisfied:

$$\|T^{(j+1)}-T^{(j)}\|\le err \tag{7}$$

where err is a given minimal error. Once the threshold $\hat{T}$ is determined, the difference image can be classified into two classes. It is worth noting that the given minimal error can be an infinitesimal value because $\{T^{(j)}\}_{j=1,2,\cdots}$ is convergent with the strictly monotonic increase (a Cauchy sequence). At convergence of the sequence, a local maximum of the aforedefined function is reached. The initial estimate $T^{(0)}$ is obtained by considering the possible extent of changed areas in the two images.

2. Determination of three classes

It is obvious that the single threshold decision procedure described in Section II.1 is subject to two kinds of errors: false positive and false negative. The false positive is pixels that are detected as changed but are actually unchanged in the ground-truth map, and similarly the false negative is the pixels that are detected as unchanged but are actually changed in the ground-truth map. Utilizing the fuzzy entropy principle, binary segmentation of the difference image can be viewed as the first step that classifies the pixels into either class $\phi_1(i,j)$ or $\phi_2(i,j)$. At the moment, we do not assign semantic meaning to the unchanged area $\phi_u(i,j)$ and the changed area $\phi_c(i,j)$, because some pixels which actually belong to $\phi_u(i,j)$ have been segmented into $\phi_c(i,j)$, and similarly, some pixels which actually belong to $\phi_c(i,j)$ have been segmented into $\phi_u(i,j)$.

Homogeneous regions are Gamma distributed in SAR image. Here we classify the pixels with the similar intensity values instead of the homogeneous region into one class, therefore the distribution of these pixels would be very close to a Gaussian distribution. After two classes $\phi_1(i,j)$ and $\phi_2(i,j)$ are obtained according to the optimum threshold $\hat{T}$, we compute the sample mean μ_1, μ_2 and the sample variance σ_1^2, σ_2^2 respectively associated with the two classes (Fig.1). The sample mean is calculated by taking the sum of all the values divided by the total number of the datum set. The sample variance is the sum of the squared deviations from their average divided by one less than the number of observations in the datum set. The confidence interval of the two classes $\phi_1(i,j)$ and $\phi_2(i,j)$ can therefore be defined as $[\mu_1-\omega\sigma_1,\mu_1+\omega\sigma_1]$ and $[\mu_2-\omega\sigma_2,\mu_2+\omega\sigma_2]$ respectively, where ω is the confidence coefficient. According to strategy one, the threshold T_1 and T_2, which further partition $\phi_1(i,j)$ into another two classes, and $\phi_2(i,j)$ into another two classes, would be determined as follows: $T_1=\mu_1+\omega\sigma_1$ and $T_2=\mu_2-\omega\sigma_2$ (Fig.1). Then two middle neighbor classes are merged into one class, which is denoted as the unlabelled class, the two other classes with the high confidence are denoted as the changed $\phi_c(i,j)$ and unchanged $\phi_u(i,j)$ respectively. Up to now, the difference image is classified into three classes: changed, unchanged, or unlabelled. The unlabelled class contains most of the ambiguous pixels that are responsible for false positive and false negative errors occurred during the classification procedure, and a voting method will be employed to process the unlabelled class in the next section.

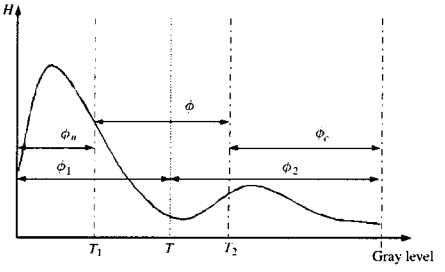

Fig. 1. Representation of our thresholding method applied to difference image

III. Classification of Unlabelled Pixels

It is well known that change detection at pixel level is very sensitive to noise since it does not exploit the contextual information. In fact, the probability that one pixel is assigned to a non-changed class or a changed class is not only influenced by its current intensity, but also continuously influenced by the intensities of its local neighboring pixels. Our objective of processing the unlabelled pixels is to predict the "real" value for each unlabelled pixel by considering the known intensity values of its local neighborhood. Here we model the interaction between pixels in the local neighborhood as a

voting procedure, and assess the saliency of each unlabelled pixel by analyzing the region configuration in the local neighborhood. Each pixel around the unlabelled pixel casts one value at its location, then the candidate pixel collects all the voting values cast at its location by all the other pixels, and the resulting value, which will replace the original intensity value of the candidate, is the sum of the voting values cast at the pixel. In addition, it is reasonable to assume that the strength of interaction between pixels in a homogeneous region decreases as the distance between them increases. This means that the farther the distance between pixels, the less the strength of their interaction. Here the Gaussian decay function is used as a weight function.

Therefore, for the ith unlabelled pixel, its "real" intensity value can be predicted by the following:

$$I_i = \sum_{j\in C} I_j \omega(d_{ij}) \Big/ \sum_{j\in C} \omega(d_{ij}) \tag{8}$$

where I_j is the intensity value of jth pixel, d_{ij} is the distance between the ith unlabelled pixel and the jth pixel, and $\omega(x) = \exp(-x^2/\sigma_2)$ is the Gaussian decay function, and the parameter σ is determined by the size of the homogeneous region C. Eq.(8) means that the intensity of the ith candidate is a weighted average of the intensity in the homogeneous region C.

As is well known, voting through replacing the pixel in the center of a window by the weighted average of the pixels in the window indiscriminately blurs the image, removing not only the noise but also salient information. Thus, the voting procedure with a homogeneous region is preferred. On the other hand, the result is dependent on the size of the homogeneous region. Intuitively, the more casts the candidate has, the more accurate is the possibility that the candidate belongs to either the unchanged or the changed class. Therefore we hope to find the largest size of the homogeneous region in which there are the most casts for each candidate pixel. Without explicit image segmentation but based on continuity of intensity uniformity, a simple and effective algorithm has been introduced to estimate the size of the homogeneous region for the candidate pixel in Ref.[22]. Firstly a circle $B_k(c)$ with center at every candidate pixel $c \in C$ and radius k was defined by: $B_k(c) = \{e \in C | \|c - e\| \le k\}$. Then they defined a function,

$$F_k(c) = \frac{\sum_{e\in B_k(c)-B_{k-1}(c)} G_\varphi(|f(c) - f(e)|)}{|B_k(c) - B_{k-1}(c)|},$$

which indicates the fraction of the set of pixels in the circle boundary whose intensities in the circle boundary are sufficiently uniform with that of c, where $|f(c) - f(e)|$ is local intensity difference for pixels (c, e), and G_φ is the zero mean unnormalized Gaussian function with standard deviation σ_φ. Finally, $F_k(c)$, the fraction of the scene containing c that is contained in the circle boundary, was iteratively checked by increasing the circle radius k by 1, starting from 1 until the largest size was determined. Refer to Refs.[10] for the detailed algorithm descriptions and choice of parameters. Once all pixels in the unlabelled class were processed by the voting procedure, we used the single thresholding method described in Section II.1 to partition the renewed unlabelled class into either unchanged or changed class. The binary image, associated with two opposite classes, changed and unchanged, was therefore produced.

IV. Identification of Water-Inundated Regions

In order to further reduce the influence of environmental conditions, speckle noise, and detect precisely water-inundated areas, based on an empirically reasonable assumption and radiometric characteristics of water bodies in SAR images, we propose some simple and effective post-processing strategies to further process the binary image.

1. Post-processing based on the empirically reasonable assumption

To test our ability to detect the change of water body from two SAR images, the images used in our experiment were acquired before and after a flood, so that one image has more water than the other. As we know, water in SAR images holds low intensity value, while non-water is usually brighter. From the first image X_1 to the second X_2, if a flood happens, the intensity value of a changed pixel or the intensity mean value of a flooded region should change from high to low. When the binary change image is mapped to the two original images $(X_k, k = 1, 2)$, for each change region, if the intensity mean value of the corresponding region in image X_1 is lower than the one in image X_2, then we think the change region is not generated by water.

In order to develop an automatic flood detection system, it is necessary to automatically determine which original image has more water. To solve the problem, we first map all the detected changes into the two original images respectively, and then compare their global intensity mean values. Since water bodies have a low intensity value in SAR images, the image whose global intensity mean value is lower can be confirmed as having more water. Then, for each detected region, the local intensity mean values of the corresponding regions in the two original images are calculated respectively. By comparing the two local mean values with the global mean values, one is able to judge whether this change region is generated by water. Consequently, some change regions that cannot be caused by water will be removed.

2. Post-processing based on statistical measurement of region

Although water bodies usually look dark and smooth in SAR images, they appear rough and relatively bright when the surface of water fluctuates because of weather conditions or some other factors. The roughness and brightness of water bodies caused by environmental noise should be considered, and the detected change owing to these factors should be excluded. Here the region correlation and entropy measurement are applied to cope with the problem.

Correlation is usually used to describe the degree of relationship between two random variables. What we expect to measure is the correlation between the intensity levels of the two regions. It can be defined as:

$$r_1 = \frac{NSI_{1i}I_{2i} - SI_{1i}SI_{2i}}{\sqrt{[NSI_{1i}^2 - (SI_{1i})^2][NSI_{2i}^2 - (SI_{2i})^2]}}, \quad \mathcal{S} = \textstyle\sum_{i\in R_{1,2}} \tag{9}$$

where N is the number of pixels in the studied region and I_{1i} and I_{2i} respectively denote pixel intensity values of the two corresponding regions $(R_{1,2})$ in the two original images. The larger r_1 is, the stronger the correlation between the two regions, and the smaller the probability that the detected region belongs to the real changed one.

The entropy, which is defined as

$$H = -\sum_{i\in\Omega} [P(x_i) \log P(x_i)],$$

can be applied to describe the homogeneity of the region in the image, where $P(x_i)$ is the probability of the occurrence of the ith intensity level x_i inside the given region Ω. For a homogeneous region, for example, if the occurrence probability of the intensity levels is uniformly distributed, then $P(x_i) = \text{const}$, for $i \in \Omega$, and H is high. In SAR images, water areas are dark and relatively smooth with some little bright areas, and their entropy is high. For a non-water region, the occurrence probability of intensity levels is usually arbitrarily distributed, and the entropy is low. Hence, this kind of statistical measurement of a water body (*i.e*, entropy) is a suitable way to discriminate water and non-water areas. When the binary change image is mapped to the two original images, the intensity levels of the corresponding regions in the image with more water should be uniform, and the intensity levels in the other image should be varied. In Section IV.1 we determined which original image has more water, *e.g.* X_1. For each detected region, if H_1

and H_2 are the entropy values in the first and second images respectively, then we have $H_2 > H_1$. Therefore, for each detected region, by comparing their entropy values in two images, one is able to determine whether the region is caused by flood.

On the other hand, for an inundated region, even though the intensity levels in two images may be similar, the entropy values are usually different due to the radiometric characteristics of water bodies. The entropy difference between two regions is written as: $r_2 = \|H_1 - H_2\|$, where H_1, H_2 are the entropy of the corresponding regions in two images. The measurement in fact represents the dissimilarity of the structural feature of the region. Obviously the larger r_2 is, the higher the possibility that the change is generated by water. Correlation measurement and entropy measurement are two different views of a region description that can complement each other. From this point of view, a better region-based verification should be based on both of them. Thus, the verification measurement can be written as: $r = \alpha(1 - r_1) + \beta r_2$, where α, β are constants that tune the influence of the two kinds of measurements on post-processing, and $\alpha + \beta = 1$. r_1 and r_2 are normalized respectively by setting their maximum values to 1. For each pair of regions, if r is lower than a given value, then the detected change is considered not to be caused by water.

Finally, due to the continuity of water bodies, the detected result that reflects change in the real scene can be modelled as connected components of small size. This means that a pixel belonging to a water body is likely to be surrounded by pixels belonging to the water body. Thus some single isolated pixels and small clusters are considered to be caused by noise, and will be removed in post-processing. Undoubtedly, this simple elimination will make some mistakes, however, one can notice from the experiment that most of the removed small clusters are caused by other factors instead of change of water body.

After post-processing, some regions with small size and unconformability to water change will be eliminated. As we know, speckle noise will result in differences of intensity between two images. The thresholding approach wrongly classifies some of the contaminated pixels into either change or no change class due to their large intensity differences, and classifies some of them into the unlabelled class due to moderate intensity difference. The voting algorithm, performed on the unlabelled pixels, is somewhat equivalent to filtering with structure detection, in which the estimate of homogeneous region (*i.e.* structure detection) makes full use of the spatial contextual information of a water body. These pixels, which otherwise cannot be labelled to a certain class, can now be classified as either changed or unchanged through the voting procedure, as discussed in Section II. 3. On the other hand, the post-processing, performed on the change image according to the radiometric features of water bodies in SAR images, improves greatly the detected result by eliminating the change regions caused by factors such as different environmental conditions, speckle noise, *etc.* Therefore, although speckle noise is not explicitly considered in this paper, the voting procedure and post-processing can effectively avoid errors caused by speckle noise.

V. Experiments

The experiments are performed using two repeat-pass ERS-2 SAR images taken from Poyang Lake, China, on Aug.24, 1996 and Aug.14, 1999. Two pairs of sub-images are extracted: one of them is impacted by a small flood (Fig.2), and the other by a big flood (Fig.7). They were co-registered with a 1.5 pixels error by our software.

Fig.2 shows the ortho-rectified and radio-metrically normalized sub-image pair of the Poyang Lake taken at different times. The difference image is calculated by taking into account the absolute difference of the pixel intensity value over two images. By processing the difference image, as discussed in Section II, we obtain the result with three classes: changed (in white), unchanged (in blue), and unlabelled classes (in red), as illustrated in Fig.3(a). Fig.3(b) shows the result after a voting procedure is applied to the unlabelled pixels, which is described in Section III. Fig.4(a) shows the final results after post-processing. When the detected change regions are mapped to one of the original images as shown in Fig.4(b), by visual comparison, one can clearly see that most of the change regions generated by water have been identified. Fig.7 is the sub-image pair with the larger flooded areas, and the experimental result is shown in Fig.8.

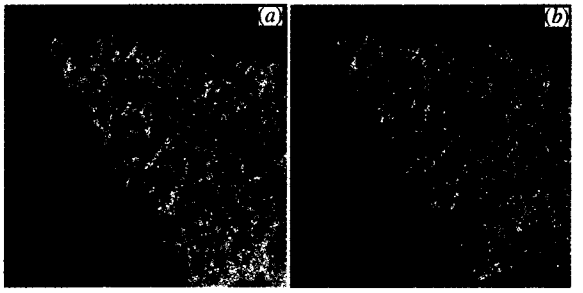

Fig. 2. Two SAR sub-images acquired on Aug.24, 1996 and Aug.14, 1999

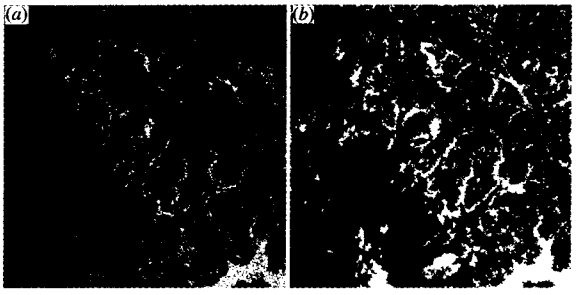

Fig. 3. (a) the difference image with three classes: the absolute unchanged one, the absolute changed one, and the unlabelled one; (b) result after a voting procedure is applied to the unlabelled class

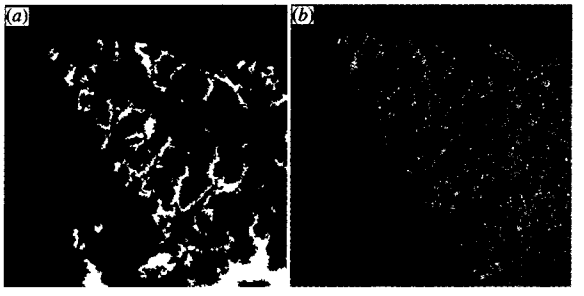

Fig. 4. (a) the final result after post-processing; (b) the detected results are mapped onto one of the original images

It is an important step to evaluate the "correctness" of the detected result. In this paper, we focus on unsupervised change detection, and the ground truth information about change regions over two images is not available. From Fig.2, one can see that it is a very difficult task even for human beings to correctly extract the regions of water in such a scene. Here we use Intelligent Scissors[8] to extract the edges of water body interactively, as shown in Fig.5(a). The ground truth can be approximately obtained by comparing the edges over the two images in Fig.5(b). If a pixel is found to be changed in both the ground truth and the detected binary image, it is considered a true positive. Fig.6 visually shows the comparative results before (a) and after (b) post-processing, and the true

positive, false positive, and false negative are in white, blue, and red respectively. The computational time is greatly dependent on the size of images used in our application. In the experiment 1, the computational time is 5.8s in the platform with Pentium 2.8G, Window XP, Memory size: 2G, Visual C++.

Fig. 5. (*a*) one of the sub-images with edge features overlaid; (*b*) the "ground truth" extracted by comparing the edges over the two images

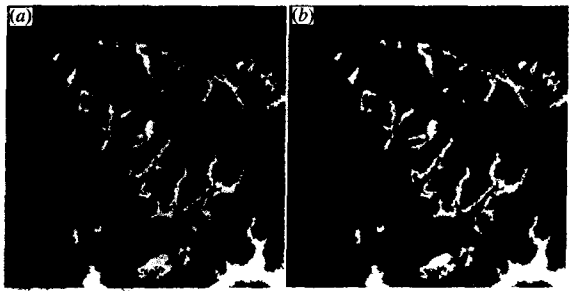

Fig. 6. The visual comparison of the detected result before (*a*) and after (*b*) post-processing: false positive, false negative, and true positive

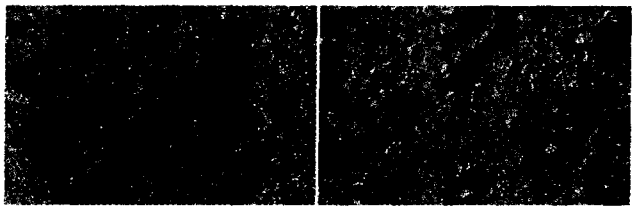

Fig. 7. Two SAR sub-images acquired at different times

Besides the visual comparison, the detected result can be compared numerically with the ground truth. A stratified systematic unaligned sample is used to select sample pixels for accuracy verification. In experiment 1, a total of 1024 pixels were sampled, with 914 unchanged pixels and 110 changed pixels in the ground truth image. In experiment 2, a total of 1200 pixels were sampled, with 1038 unchanged pixels and 162 changed pixels. The change error matrix is usually used in error analysis of change detection. Table 1 illustrates the change error matrix before and after the post-processing verification. If the detection accuracy is defined as the number of correctly classified pixels (true positive) with respect to the total number of ground truth pixels, and the False positive (FP) and False negative (FN) error rates are respectively defined as the number of false positive and false negative pixels with respect to the number of ground truth pixels, then in experiment 1, the false positive and false negative error rates were 39.1% and 16.3% respectively and the detection accuracy was 83.6% before post-processing. After post-processing, the respective rates were 14.5%, 18.2%, and 81.8%. Table 3 illustrates the resultant errors of the two experiments before and after post-processing. Although post-processing eliminates some correctly classified pixels (the final detection accuracy is a little lower than the one before post-processing, and the false negative error rate is a little higher), as a whole, it improves significantly the detected result (the false positive error rate greatly drops).

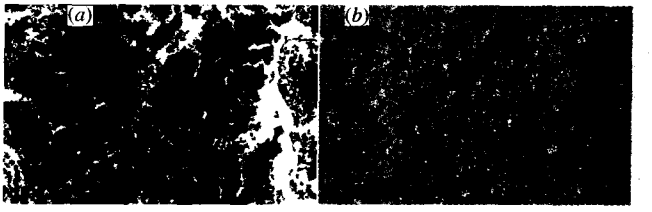

Fig. 8. (*a*) the final result after verification; (*b*) the detected change regions are mapped in one of the two images

Table 1. The error matrix in experiment 1: the ground truth is in the first column, and the detected results before and after post-processing are in the rows to the right

Experiment 1		Detected result			
		Before post-processing		After post-processing	
Ground truth		Unchanged	Changed	Unchanged	Changed
Unchanged	914	871	43	898	16
Changed	110	18	92	20	90
Total	1024	889	135	918	106

Table 2. The error matrix in experiment 2: the ground truth is in the first column, and the detected results before and after post-processing are in the rows to the right

Experiment 2		Detected result			
		Before post-processing		After post-processing	
Ground truth		Unchanged	Changed	Unchanged	Changed
Unchanged	1038	993	45	1012	26
Changed	162	33	129	34	128
Total	1200	1026	174	1046	154

Although the above comparative analysis confirms the effectiveness of the verification technique, which significantly improves the accuracy of the change-detection map and meanwhile reduces the noise in this binary map, the false positive and false negative errors are still a little high. The main reason is that water bodies at different seasons have different radiometric characteristics due to various pollution, speckle noise, etc. Although the post-processing of the difference image described in this paper greatly improves the detected result, the problem is not fully solved. Additionally, the "ground truth" is manually extracted and not so accurate in this case.

Table 3. The accuracy analysis before and after post-processing

	Experiment 1		Experiment 2	
	Before post-pro.	After post-pro.	Before post-pro.	After post-pro.
FN rate (%)	16.3	18.2	20.4	20.9
FP rate (%)	39.1	14.5	27.8	16.0
Accuracy (%)	83.6	81.8	79.6	79.0

VI. Conclusions

We have presented a unifying computational framework for the unsupervised change detection of flooded areas in SAR images, and have given the related experimental results and result analysis. Our methodology can be grounded on three complementary

aspects: a thresholding approach based on the fuzzy entropy principle is proposed to partition the difference image into three classes: unchanged, changed, and unlabelled. By exploiting the spatial contextual information of the difference image, a voting procedure is applied to process the unlabelled pixels. Further improvements in the change-detection accuracies are obtained by making full use of the radiometric properties of water bodies in SAR images. The significant advantage of our approach is reflected in the fact that our approach allows us to detect automatically the change regions of flooding in two SAR images without any prior information about the floods.

References

[1] L. Bruzzone and D.F. Prieto, "Automatic analysis of the difference image for unsupervised change detection", *IEEE Trans. on Geoscience and Remote Sensing*, Vol.38, pp.1171–1182, 2000.

[2] F. Bujor, E. Trouve *et al.*, "Application of log-cumulants to the detection of spatio-temporal discontinuities in multi-temporal SAR images", *IEEE Trans. on Geoscience and Remote Sensing*, Vol.42, pp.2073–2084, 2004.

[3] M.J. Carlotto, "Detection and analysis of change in remotely sensed imagery with application to wide area surveillance", *IEEE Trans. on Image Processing*, Vol.6, pp.189–202, 1997.

[4] Jr. P.S. Chavez and D.J. MacKinnon, "Automatic detection of vegetation changes in the southern untied states using remotely sensed images", *Photogram. Eng. Remote Sensing*, Vol.13, pp.1285–1294, 1994.

[5] T. Hame, I. Heiler *et al.*, "An unsupervised change detection and recognition system for forestry", *International Journal of Remote Sensing*, Vol.19, pp.1079–1099, 1998.

[6] T. Kasetkasem and P.K. Varshney, "An image change detection algorithm based on Markov random field models", *IEEE Trans. on Geoscience and Remote Sensing*, Vol.40, pp.1815–1823, 2002.

[7] K.R. Merril and L. Jiajun, "A comparison of four algorithms for change detection in an urban environment", *Remote Sensing Environment*, Vol.63, pp.95–100, 1998.

[8] E.N. Mortensen and W.A. Barrett, "Intelligent scissors for image composition", *In Proceeding of SIGGRAPH'95*, pp.191–198, Los Angeles, USA, 1995.

[9] S.K. Pal, "Fuzzy image processing and recognition: uncertainty handling and applications", *International Journal of Image and Graphics*, Vol.1, pp.169–195, 2001.

[10] P.K. Saha *et al.*, "Optimum image thresholding vis class uncertainty and region homogeneousity", *IEEE Trans. on Pattern Analysis and Machine Intelligence*, Vol.23, pp.689–706, 2001.

[11] P.K. Sahoo, S. Soltani, A.K.C. Wong and Y. Chen, "A survey of thresholding techniques", *Computer Vision, Graphics, Image Processing*, Vol.41, pp.233–260, 1988.

[12] X.R. Li, F.C. Wu and Z.Y. Hu, "Convergence of a mean shift algorithm", *Journal of Software* (in Chinese), Vol.16, No.3, pp.265–274, 2005.

PAN Chunhong received his B.S. degree in automatic control from Tsinghua University, Beijing, China, in 1987, his M.S. degree in 1990, and his Ph.D. degree in pattern recognition and intelligent system from Institute of Automation, Chinese Academy of Sciences in 2000. He worked on computer vision at University of Southern California in USA for one year as a visiting researcher in 2001. He was a visiting scientist at Ecole Nationale Superieure des Telecommunications (ENST), France from Nov. 2005 to Feb. 2006. Now he is working as an associate professor at the National Laboratory of Pattern Recognition of Institute of Automation, Chinese Academy of Sciences. His research interests lie in computer vision, pattern recognition, and remote sensing. (Email: chpan@nlpr.ia.ac.cn)

PRINET Veronique received her Ph.D. degree in 1999 from University Paris-11 Orsay. Her research work being hold at INRIA (French National Institute in Computer Sciences and Automation), in collaboration with CNES (French National Center for Spatial Studies). Currently she is an associate professor at the National Laboratory of Pattern Recognition of Institute of Automation, Chinese Academy of Sciences. Her research activities focus on image understanding, pattern/objectrecognition, probabilistic modeling, low level features extraction, deformation/change analysis.

YANG Qing is a professor in the National Laboratory of Pattern Recognition at the Institute of Automation, Chinese Academy of Sciences. He was a computer scientist in Computing Sciences at Lawrence Berkeley National Laboratory, USA from 1999 to 2004. He received Ph.D. degree in computer science from the Institute of Automation, Chinese Academy of Sciences. His current research interests include image processing, pattern recognition, and bioinformatics.

MA Songde received the B.S. degree in automatic control from Tsinghua University, China, in 1968. He received the Ph.D. degree in 1983 and the "Doctoral d'Elat es Science" degree in 1986 from University of Paris 6 in image processing and computer vision. He was an invited researcher in the computer vision laboratory of the University of Maryland, College Park, in 1983. He was a researcher at the robot vision laboratory of INRIA, France, from 1984 to 1986. Since 1986, he has been a professor at the National Laboratory of Pattern Recognition of Institute of Automation, Chinese Academy of Sciences. He was the president of the Institute of Automation of Chinese Academy of Sciences in 1996–2000. He obtained the Best Paper Award and Best Technique Award in Eurographic'85 and the Outstanding Young Scientist Award of Chinese Academy of Sciences in 1989. His research interests include computer vision, computer graphics, pattern recognition, and robotics. Dr. Ma has been the vice-minister of the Ministry of Science and Technology (MOST) of China since April 2000.